Thermodynamic Consistency in Microkinetic Development of Surface Reaction Mechanisms

A. B. Mhadeshwar,[†,‡] H. Wang,[‡,§] and D. G. Vlachos*[,†,‡]

Department of Chemical Engineering, Department of Mechanical Engineering, and Center for Catalytic Science and Technology (CCST), University of Delaware, Newark, Delaware 19716-3110

Received: April 9, 2003; In Final Form: August 13, 2003

The foundation of microkinetic analysis over 10 years ago has drastically changed the way of parametrization of rates of surface-catalyzed reactions. In the initial stages of development, some parameters arose from experimental data whereas others were fitted to experimental data. Semiempirical and first principles quantum mechanical and statistical mechanics simulations nowadays are powerful tools in estimating kinetic parameters. However, even in best cases, some tuning of parameters is typically necessary for quantitative model predictions. During this process, parameters of reaction mechanisms may violate thermodynamics. Here we review thermodynamic constraints of reaction networks and derive expressions applicable to surface reactions. We present three examples of ethylene hydrogenation, ammonia synthesis, and hydrogen oxidation to assess the thermodynamic validity of literature mechanisms. Various methods to ensure thermodynamic consistency are discussed and demonstrated with a specific example of H_2 oxidation on Pt. The use of semiempirical techniques, such as the bond order conservation (BOC), known also as unity bond index-quadratic exponential potential (UBI-QEP) or Polanyi free energy relations, and first principles density functional theory (DFT), in conjunction with fitting of experimental data is discussed. Finally, mechanisms compatible with Surface CHEMKIN are proposed.

Introduction

Microkinetic analysis has evolved into a promising tool for modeling surface reactions. Bush and Dyer[1] appear to be the first to employ this analysis. They presented detailed reaction mechanisms, without assuming a rate-determining step (RDS), and optimized the preexponential factors and activation energies against experimental data using a least-squares minimization technique. Microkinetic analysis of surface reaction mechanisms has been well established by Dumesic and co-workers.[2] A review of more recent work can be found in refs 3 and 4.

A key advantage of the microkinetic analysis is that a mechanism developed at certain conditions is expected, in many cases, to capture system features under significantly different conditions. The analysis involves setting up a network of elementary reactions, which capture the essential features of surface-catalyzed chemistry. Typical assumptions about an RDS, most abundant reaction intermediate (MARI), quasi-steady state (QSS), partial equilibrium (PE), etc. are avoided, because with changing operating conditions the validity of these assumptions cannot be verified a priori. Instead, the species concentrations are solved rigorously, using in most cases, numerical methods. In addition to the mean field approach usually employed in microkinetic analysis, spatial nonuniformity can be considered by using kinetic Monte Carlo simulations. See, for example, refs 5−10 for recent work in this area.

A major challenge in microkinetic analysis is the estimation of reaction rate parameters. Approaches of rate estimation can be broadly classified into four categories, viz. first principles simulations, semiempirical methods, the hybrid approach, and a purely experimentally based approach. First principles simulations using ab initio quantum chemistry methods (e.g., density functional theory (DFT)), transition state theory (TST), and statistical mechanics can be used to estimate the reaction rate parameters. Excellent reviews on the application of DFT in heterogeneous catalytic reactions have been given by van Santen and Neurock,[11] and Norskov.[12] Application of statistical mechanical principles is common for estimation of preexponential factors.[2,13,14]

Predictive reaction mechanisms can also be developed by using semiempirical techniques, such as bond order conservation (BOC), generalized in 1998 to be known as unity bond index-quadratic exponential potential (UBI-QEP),[15,16] Polanyi relationships,[17,18] and electronegativity scales in combination with some fitting (see, for example, refs 10, 19, and 20). Using a combination of the UBI-QEP and TST (for order of magnitude estimates of preexponential factors) followed by a systematic optimization of key preexponentials against experimental data, Aghalayam et al. developed predictive surface reaction mechanisms for the oxidation of H_2,[21] CO,[22] and CH_4.[23,24]

The hybrid theoretical approach consists of a combination of semiempirical techniques with DFT-based heats of chemisorption or reaction energetics in the zero coverage limit and UBI-QEP to account for adsorbate−adsorbate interactions for all steps.[8,9,25−27] In addition, TST is used to obtain an order-of-magnitude estimate for the preexponential factors.[2] Finally, the experimentally based approach involves extraction of rate parameters from individual surface science experiments, such as temperature-programmed desorption (TPD), and in some cases, an optimization of the remaining rate parameters in a proposed reaction network against targeted experimental data.[28−31]

* Corresponding author. Tel.: (302) 831-2830. Fax: (302) 831-2085. E-mail: vlachos@che.udel.edu

[†] Department of Chemical Engineering.

[‡] Center for Catalytic Science and Technology.

[§] Department of Mechanical Engineering.

10.1021/jp034954y CCC: $25.00
Published on Web 10/16/2003

Rate parameters estimated by following the approaches outlined above have their intrinsic uncertainties. For example, activation energies of surface reactions computed using DFT have an accuracy of ~5 kcal/mol.[9,11] Given these uncertainties, a reaction mechanism consisting of individually estimated rate parameters is usually unable to quantitatively describe experimental data. Furthermore, issues related to the heterogeneity of real catalysts, such as point defects and steps of facets, multiple facets, and edges and corners of sites of supported catalysts render first principles predictions of reaction parameters of surface processes very difficult. We therefore expect that adjustments of kinetic parameters are always necessary and these adjustments are usually carried by systematic optimization of kinetic parameters against experimental data. This is the case even for gas-phase reaction mechanisms, whose development is considerably more advanced than that of the surface reaction mechanisms.

In mechanism development and rate parameter fitting or optimization, an issue often overlooked is thermodynamic consistency at both the enthalpic and entropic levels. The origin of the problem has been the lack of thermochemical data for surface species, and as such, the rate parameters of forward and backward reactions are often chosen in an ad hoc fashion without considering thermochemical constraints imposed upon these parameters. This issue has been brought up in several instances,[2,3,21,32] but there is no strategy available for testing and ensuring thermodynamic consistency of an arbitrary complex reaction network. As a result, although a few published mechanisms are thermodynamically consistent, most literature mechanisms are not.

What are some ramifications of violating thermodynamic consistency? Enthalpic inconsistency gives incorrect solutions to the energy conservation equation. Error in the computed temperature, in turn, translates to incorrect predictions of heat exchange and conversion/selectivity in nonisothermal simulations. In case of isothermal simulations as well, errors appear through the calculation of rates in mass balance, thus yielding incorrect conversion/selectivity. Entropic inconsistency directly translates to fundamental inconsistency in the preexponential factors. Finally, entropic and enthalpic inconsistency distorts the underlying equilibrium constant, which affects the prediction of equilibrium states.

Limited attempt has been made previously to ensure thermodynamic consistency in a reaction mechanism or for individual reaction steps. In a microkinetic analysis of hydroisomerization of *n*-hexane, van Santen and co-workers[33] determined the preexponential factors of adsorption steps from those of desorption steps and the equilibrium adsorption data on zeolites. Energetics for the surface reaction steps was estimated such that the complete energy diagram was consistent. This approach, though highly desirable, is limited by the availability of a thermodynamic database of specific heats, which is rare for the case of surface species. In their modeling study of methane dimerization on Li/MgO, Aparacio et al.[34] made an attempt to ensure thermodynamic consistency of the rate parameters. Activation energies and preexponential factors of two steps in the proposed mechanism were modified to correctly reproduce the enthalpy and Gibbs free energy of the overall reaction process. In a study of the water-gas shift reaction on Mo/Al_2O_3, Lund et al.[13] estimated the entropy of adsorption following statistical mechanical principles. When the preexponential factors of forward reactions were estimated by the TST, the preexponential factors of backward reactions were determined using the entropy of adsorption. The heats of chemisorption and the parameters in the Polanyi relationship were considered as adjustable parameters to make the model predictive.

In this paper, we review the criteria of thermodynamic consistency and demonstrate cases of thermodynamic inconsistency in previously published reaction mechanisms. We then present a methodology that ensures thermodynamic consistency of the entire mechanism. Our approach is conceptually similar to those just discussed, but it is more systematic than any previously used methods. We present a proof-of-concept analysis using the reaction model of H_2 oxidation on Pt as an example.

Thermodynamic Consistency

Consider a collection of reactions

$$R_i = \sum_{k=1}^{K} \nu_{ik} B_k \qquad i = 1, ..., I \tag{1}$$

where B_k is the kth species, ν_{ik} is the stoichiometric coefficient of the kth species of the ith reaction, and I and K are the numbers of reactions and species, respectively. Here, B_k can be a surface or a gaseous species, as one may find both types of species in adsorption−desorption and Eley-Rideal reaction steps. For elementary reactions, the reaction rate constant is typically described through the Arrhenius law

$$k_i^{\mathrm{f,b}} = A_i^{\mathrm{f,b}} \mathrm{e}^{-E_i^{\mathrm{f,b}}/RT} \tag{2}$$

where f and b stand for the forward and backward steps, A is the preexponential factor, E is the activation energy, R is the ideal gas constant, and T is the temperature. Sticking coefficients and preexponential factors are hereafter termed as prefactors.

The equilibrium constant of the ith reaction is given in terms of the Gibbs free energy ΔG_i of the reaction as

$$K_i^{\mathrm{eq}} = \mathrm{e}^{-\Delta G_i/RT} = \mathrm{e}^{\Delta S_i/R} \mathrm{e}^{-\Delta H_i/RT} = K_i^{\mathrm{eqS}} K_i^{\mathrm{eqH}} \tag{3}$$

where ΔS_i and ΔH_i are the entropy change and enthalpy change of the reaction, respectively, and K_i^{eqS} and K_i^{eqH} are the entropy and enthalpy components of the equilibrium constant, respectively. Obviously, we have

$$E_i^{\mathrm{f}} - E_i^{\mathrm{b}} = \Delta H_i \tag{4a}$$

and

$$A_i^{\mathrm{f}}/A_i^{\mathrm{b}} = \mathrm{e}^{\Delta S_i/R} \tag{4b}$$

Equations 4a and 4b form the basis of the enthalpic and entropic constraints.

Sellers and Shustorovich note that "The general meaning of eq 4a is that the difference between the Arrhenius activation barriers is the temperature-dependent enthalpy change for the reaction".[35] Specifically, eq 4a can be expanded into

$$E_i^{\mathrm{f}} - E_i^{\mathrm{b}} = \Delta H_i^0 + \sum_{k=1}^{K} \nu_{ik} H_k(T) \tag{5a}$$

where ΔH^0 is the standard-state enthalpy of reaction, and $H_k(T)$ is the sensible heat of species k relative to 298 K. To a first approximation, the sensible heat term in eq 5a is linear in T.[36] A quadratic expression is also possible. A similar idea of temperature-dependent activation energy is proposed in Goodson et al.[37]

The activation energies E^f and E^b in eq 4a are hereafter treated as effective activation energies, and for simplicity in parametrization, they incorporate the effect of temperature on the heat of reaction. This consideration is important, as in many cases the variation of the sensible heat is not negligible. For example, the activation energy of $NO_2 \rightarrow NO + O$ varies from 72 kcal/mol at low temperatures to 42 kcal/mol at high temperatures.[36] Due to different microconfigurations of adsorbates on the catalyst, effective activation energies in Monte Carlo simulations of the same reaction step (e.g., CO* + O*) can also vary with temperature.[9,25]

Similarly, ΔS_i in eq 4b is also intrinsically dependent on temperature. In terms of the standard-state entropy of reaction ΔS_i^0, eq 4b can be expanded to

$$A_i^f/A_i^b = e^{\{\Delta S_i^0 + \sum_{k=1}^{K} \nu_{ik}[S_k(T) - S_k(298K)]\}/R} \tag{5b}$$

Thermodynamic Constraints and Reaction Basis Set. The thermodynamic constraints are manifested at two different levels. At the level of an individual reaction, enthalpic and entropic consistency can be easily satisfied, and in fact, this consistency is utilized to compute, for example, the heat of surface reactions or the activation energy of the backward reaction. However, ensuring the above consistency does not guarantee consistency for the entire reaction mechanism. Therefore, at the level of reaction mechanism, thermodynamic consistency of the rate parameters of relevant reactions needs to be carefully examined, as will be discussed below, unless the thermodynamic properties are known for each species involved in the mechanism.

Enthalpy and entropy are state functions, so any linear combination of these functions of elementary steps must also obey the same consistency at the level of an individual reaction, whether it is elementary or global. A practical problem may be that in a large reaction mechanism, there could be numerous linear combinations of reactions, which makes it a daunting task to thoroughly check and satisfy the underling thermodynamic constraints of the involving rate parameters. This difficulty is, however, removed with the approach proposed below.

Consider a set of linearly independent reactions of size L in a reaction mechanism consisting of I number of reactions ($L \leq I$). The set of linearly independent reactions forms a basis in the reaction network (the term is used here in a mathematical sense). For simplicity, we re-order the reactions such that the first L number of reactions $\{R_j\}_{i=1}^{L}$ are linearly independent. The basis set is usually not unique but its size L is unique. The nonuniqueness of the basis set is inconsequential insofar as thermodynamic consistency is concerned. Determination of the basis set involves the computation of the rank of the reaction stoichiometric coefficient matrix $[\nu_{ik}]$ through elementary operations of linear algebra,[38−40] as discussed in Appendix A.

The rest of the reactions are linear combinations of the basis set. They are termed linearly dependent reactions of the network and can be written as

$$R_i = \sum_{j=1}^{L} c_{ij} R_j \qquad i = L+1, ..., I \tag{6}$$

where c_{ij} are the coefficients of linearly decomposed reaction R_i onto the reaction basis. Parenthetically, although L reactions are thermodynamically independent, all I reactions may be relevant and could be included in the mechanism as long as they describe different reaction paths and obey certain kinetics rules (see, for example, ref 41 for some of these rules). This is a common point of confusion.

As a result of eq 6, the heat and entropy of a linearly dependent reaction are linear combinations of those of the reaction basis. The fact that heats and entropies of reactions are intimately related to the activation energies and prefactors, via eqs 4a and 4b, imposes constraints on the activation energies and prefactors of the linearly dependent reactions. Specifically, the activation energy and prefactor of a linearly dependent reaction must satisfy

$$E_i^f - E_i^b = \Delta H_i = \sum_{j=1}^{L} c_{ij} \Delta H_j = \sum_{j=1}^{L} c_{ij} (E_j^f - E_j^b) \qquad i = L+1, ..., I \tag{7}$$

$$\ln(A_i^f/A_i^b) = \frac{\Delta S_i}{R} = \sum_{j=1}^{L} c_{ij} \frac{\Delta S_j}{R} = \ln \prod_{j=1}^{L} (A_j^f/A_j^b)^{c_{ij}} \qquad i = L+1, ..., I \tag{8}$$

Equations (7) and (8) define the underlying thermodynamic constraints at the level of a reaction mechanism.

Special Reaction Basis for Surface Reaction Mechanisms. The above discussion applies to any reaction mechanism, independent of the phase. Next we shall focus our discussion on surface reaction mechanisms. Suppose that K_s surface species exist in a K-species mechanism (the rest, $K - K_s$, are gaseous species). A key issue in the thermodynamic consistency of surface reaction mechanisms is that the heats of surface reactions are linear combinations of heats of formation of surface species and heats of analogous gas-phase reactions. The same is valid for entropy as well. Therefore, if one ensures thermodynamic consistency of the basis set of L surface reactions, the rest of the reactions should be linear combinations of the basis set. In other words, the number of linearly independent reactions is typically equal to the number of surface species, i.e., $L = K_s$.

The specific reaction steps chosen as linearly independent are arbitrary. However, we prefer to use the reversible adsorption−desorption steps as the basis set, even if some of these steps might not be directly included in the mechanism. Note that when two adsorption steps exist in the mechanism leading to the same surface species, e.g., H + * = H* and H_2 + 2* = 2H*, where H* is the surface species, only one of the two paths belongs to the basis. On the other hand, if one considers physisorption of H_2, H_2 + * = H_2*, and also the dissociative adsorption of H_2, H_2 + 2* = 2H*, then one has to consider both steps in the basis as there are two relevant species. This choice is dictated by the fact that the heats of chemisorption and activation energies of desorption are more readily available from microcalorimetry and TPD, respectively, than the activation energies of surface reactions. Furthermore, heats of chemisorption have been tabulated or can be readily estimated using UBI-QEP. Finally, computation of heats of chemisorption via DFT is generally easier than determining activation energies of surface reactions.

After choosing the basis, we propose the following method to ensure thermodynamic consistency of surface reaction mechanisms. For every surface reaction step R_i^{surf} in the mechanism that does not belong to the basis, an analogous gas-phase reaction R_i^{gas} is written. This analogous gas-phase reaction can be viewed as a linear combination of the surface step plus adsorption steps $R_{k'}$ of the surface species k' involved

$$R_i^{gas} = R_i^{surf} - \sum_{k'=1}^{L} \nu_{ik'} R_{k'} \qquad i = L+1, ..., I \tag{9}$$

TABLE 1: Assessment of Literature Surface Reaction Mechanisms for Thermodynamic Consistency[a]

	ΔH^{gas} (kcal/mol)	ΔS^{gas} (eu)	ΔG^{gas} (kcal/mol)	K^{eqH}	K^{eqS}	K^{eq}
C_2H_4 Hydrogenation Mechanism by Rekoske et al.[30] at 300 K ($I=5$, $K=7$, $L=4$)						
Overall Reaction: $C_2H_4 + H_2 \leftrightarrow C_2H_6$						
gas-phase thermochemistry	−32.6	−29	−23.9	5.6×10^{23}	4.8×10^{-7}	2.7×10^{17}
eqs 10b & 11b						
S type site	−32.8	8.6	−35.4	7.9×10^{23}	7.5×10^{1}	5.9×10^{25}
* type site	−32.7	3.0	−33.7	7.4×10^{23}	4.6×10^{0}	3.4×10^{24}
NH_3 Synthesis Mechanisms by Bowker et al.[43,44] at 723 K ($I=7$, $K=9$, $L=6$)						
Overall Reaction: $N_2 + 3H_2 \leftrightarrow 2NH_3$						
gas-phase thermochemistry	−25.3	−55	14.2	4.4×10^{7}	1.1×10^{-12}	4.9×10^{-5}
eqs 10b & 11b						
case 1	−25.8	−56	14.8	6.1×10^{7}	5.5×10^{-13}	3.4×10^{-5}
case 2	−25.9	−56	14.6	7.0×10^{7}	5.5×10^{-13}	3.9×10^{-5}
NH_3 Synthesis Mechanism by Stoltze and Norskov [46−49] at 723 K ($I=7$, $K=9$, $L=6$)						
Overall Reaction: $N_2 + 3H_2 \leftrightarrow 2NH_3$						
gas-phase thermochemistry	−25.3	−55	14.2	4.4×10^{7}	1.1×10^{-12}	4.9×10^{-5}
eqs 10b & 11b	−25.4	−55	14.1	4.7×10^{7}	1.2×10^{-12}	5.5×10^{-5}
H_2 Oxidation Mechanism by Aghalayam et al. [21] at 1450 K, $I=9$, $K=10$, $L=4$						
Linearly Dependent Reaction: $O_2 \leftrightarrow 2O$						
gas-phase thermochemistry	121.3	32	75.5	5.0×10^{-19}	8.1×10^{6}	4.0×10^{-12}
eqs 10b & 11b	119.0	17	93.9	1.1×10^{-18}	6.1×10^{3}	6.9×10^{-15}
Linearly Dependent Reaction: $H_2O \leftrightarrow H + OH$						
gas-phase thermochemistry	122.4	31	77.4	3.5×10^{-19}	6.2×10^{6}	2.1×10^{-12}
eqs 10b & 11b	119.2	19	91.6	1.1×10^{-18}	1.5×10^{4}	1.5×10^{-14}
Overall Reaction: $2H_2 + O_2 \leftrightarrow 2H_2O$						
gas-phase thermochemistry	−119.4	−27	−79.9	1.0×10^{18}	1.1×10^{-6}	1.1×10^{12}
eqs 10b & 11b	−115.5	−22	−83.5	2.6×10^{17}	1.5×10^{-5}	3.9×10^{12}

[a] Three different systems, viz. ethylene hydrogenation,[30] ammonia synthesis,[43−49] and hydrogen oxidation,[21] are considered.

where the summation extends over all surface species (prime hereafter denotes surface species). We call such a linear combination a reaction cycle.

Consider the example of H and O combination to form OH in the gas-phase and on a surface. The surface reaction H* + O* ↔ OH* + * has H + O ↔ OH as its analogous gas-phase reaction. The relevant thermodynamic cycle can be written as

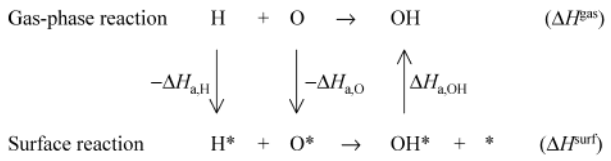

where ΔH_a is the heat of desorption (a positive quantity). A thermodynamic path analysis yields

$$\Delta H^{surf} + \Delta H_{a,OH} - \Delta H_{a,H} - \Delta H_{a,O} = \Delta H^{gas}$$

which can be generalized to

$$\Delta H_i^{surf} + \sum_{k'=1}^{L} \nu_{ik'} \Delta H_{a,k'} = \Delta H_i^{gas} \qquad i = L+1, ..., I \qquad (10a)$$

The activation energies of the surface reactions are then constrained according to

$$E_i^{f,surf} - E_i^{b,surf} - \sum_{k'=1}^{L} \nu_{ik'} (E_{a,k'} - E_{d,k'}) = \Delta H_i^{gas} \qquad i = L+1, ..., I \quad (10b)$$

where the subscripts "a" and "d" refer to adsorption and desorption, respectively. Following a similar analysis, one obtains for the entropy

$$\Delta S_i^{surf} + \sum_{k'=1}^{L} \nu_{ik'} \Delta S_{a,k'} = \Delta S_i^{gas} \qquad i = L+1, ..., I \qquad (11a)$$

In terms of prefactors, one has

$$\ln(A_i^{f,surf}/A_i^{b,surf}) - \ln \prod_{k'=1}^{L} (A_{a,k'}/A_{d,k'})^{\nu_{ik'}} = \Delta S_i^{gas} \qquad i = L+1, ..., I \quad (11b)$$

Examples of Thermodynamic Consistency

The above discussion outlined the approach to ensuring thermodynamic consistency at the level of an entire surface reaction mechanism. Here we discuss the thermodynamic consistency of several literature surface reaction mechanisms. Because the number of reactions in these mechanisms is usually large, only selected reactions are discussed (see Table 1). Most of the reactions shown in the table are linear combinations of elementary steps, and they are important for calculating the equilibrium conversion.

Ethylene Hydrogenation on Pt: Overall Reaction $C_2H_4 + H_2 \leftrightarrow C_2H_6$. Rekoske et al.[30] presented a 14-step (7 reversible reaction steps) surface reaction mechanism for ethylene hydrogenation. This is a version of the Horiuti−Polanyi mechanism,[42] modified to capture the feature of the experimental data, including steady-state kinetics, isotope tracing, and temperature-programmed reaction (TPR) results. In this mechanism, H_2 adsorbs on two types of sites (S type and * type), and each

type of sites has 5 reversible reactions ($I = 5$). For the * type, for example, the 5 reaction steps are (note that S′ is another type of site present in the mechanism)

$$C_2H_6 + 2* + S' \leftrightarrow C_2H_5** + HS' \quad \text{(R1)}$$

$$C_2H_5** + S' \leftrightarrow C_2H_4** + HS' \quad \text{(R2)}$$

$$C_2H_4** \leftrightarrow C_2H_4 + 2* \quad \text{(R3)}$$

$$HS' + * \leftrightarrow H* + S' \quad \text{(R4)}$$

$$2H* \leftrightarrow H_2 + 2* \quad \text{(R5)}$$

with 6 species ($K = 7$), among which 4 are surface species ($K_s = L = 4$).

For this particular reaction mechanism, thermodynamic consistency may be examined without invoking an analysis of linear independency among reactions. Specifically, a sum of the 5 elementary reactions yields an overall reaction

$$C_2H_4 + H_2 \leftrightarrow C_2H_6$$

Thermodynamically, the enthalpy of the above reaction is related to those of reactions R1−R5 and their activation energies, i.e.,

$$\Delta H = \Delta H_1 + \Delta H_2 + \Delta H_3 + 2\Delta H_4 + \Delta H_5$$
$$= (E_1^f - E_1^b) + (E_2^f - E_2^b) + (E_3^f - E_3^b) + 2(E_4^f - E_4^b) + (E_5^f - E_5^b)$$

Therefore, if the activation energies assigned to reactions R1−R5 are thermodynamically consistent, the ΔH value would be in close agreement with the value calculated from the gas-phase thermochemical data of C_2H_4, H_2, and C_2H_6, which are believed to be accurate. Similar argument can be made for entropy.

Using the GRI-Mech thermochemical database, we calculated the ΔH value to be −32.6 kcal/mol at 300 K, as seen in Table 1. Based on the activation energies, the ΔH value is −32.7 kcal/mol for the * type and −32.8 kcal/mol for the S type, both of which are in excellent agreement with the value based on gas-phase thermochemistry. This simple test shows that the mechanism appears to be thermodynamically consistent at the enthalpic level.

The same consistency, however, does not extend to entropy. As shown in Table 1, the entropy change of the overall reaction should be −29 eu on the basis of gas-phase thermochemistry, yet the prefactors of the five reactions give a ΔS value of 8.6 eu for the S type and 3.0 eu for the * type. This discrepancy causes the equilibrium constant to be in error by 7−8 orders of magnitude! This means that one or more prefactors must be in error.

The above example has only one degree of freedom; i.e., only one elementary reaction is linear dependent. More specifically, among the 5 reaction steps (for each type of site), any 4 are linearly independent (because $L = 4$). Therefore, the inconsistency seen in the overall reaction just discussed must also be reflected using linearly independent reactions (from the thermodynamic point of view, one could substitute the linearly dependent elementary reaction with the overall one). Considering the * type, reactions R2−R5 were chosen as linear-independent reactions, and (R1) is then the dependent reaction. An analysis using eq 10b shows that $\Delta H_1 = -17.5$ kcal/mol, which is consistent with the difference in the activation energies of the same reaction, $\Delta H_1 = E_1^f - E_1^b = -17.7$ kcal/mol. On the other hand, the entropy change is −5.4 eu, as calculated using eq 11b, yet the prefactors of reaction R1 indicate that $\Delta S_1 = 32.1$ eu.

Ammonia Synthesis on Fe: Overall Reaction $N_2 + 3H_2 \leftrightarrow 2NH_3$. Another example is ammonia synthesis on an iron catalyst, a commercial process typically operated near 723 K and 100 atm. Bowker et al.[43,44] proposed two reaction mechanisms, denoted here as cases 1 and 2. These mechanisms were used by Dumesic and Trevino[45] to evaluate the performance of an industrial reactor. For both cases, there are 7 reversible reactions ($I = 7$), a total of 9 species ($K = 9$), and 6 surface species ($K_s = L = 6$). Out of the 7 reaction steps, 6 steps are found to be linearly independent. Table 1 shows the enthalpy and entropy calculated from the gas-phase thermochemical data and from eqs 10b and 11b for the overall reaction $N_2 + 3H_2 \leftrightarrow 2NH_3$, which was obtained, again, by summing the elementary reactions. It is seen that the mechanisms appear to be thermodynamically consistent at both the enthalpic and entropic levels.

A similar reaction mechanism was proposed by Stoltze and Norskov[46−49] and also used by Dumesic and Trevino[45] for plug flow reactor modeling. Stoltze and Norskov estimate the rate constants of adsorption and desorption steps, using data obtained on Fe single crystals at ultrahigh vacuum.[50] The TPD spectra were used to determine the ground-state energies of species such as N*, H* and NH_3*. The activation energies of hydrogenation steps were approximated from estimates of relative stabilities of the various NH_x* species. When a similar analysis is performed for this mechanism, it is observed that this set is thermodynamically consistent at 723 K in terms of both enthalpy and entropy, as seen in Table 1.

A common feature of the examples illustrated above is that the mechanism in question has only one degree of freedom. Therefore thermodynamic consistency can be easily achieved with the adjustment of the parameters of a single reversible reaction step. This feature is quite uncommon, as in many cases the number of reactions far exceeds the number of species. In that case, the degrees of freedom become large, and ensuring thermodynamic consistency is not a trivial task. The following example illustrates this problem.

Hydrogen Oxidation on Pt: Overall Reaction $2H_2 + O_2 \leftrightarrow 2H_2O$. Here we discuss an example of H_2 oxidation on Pt on the basis of our previous work. Aghalayam et al.[21] optimized the surface reaction mechanism against experimental ignition and laser-induced fluorescence (LIF) data. Heats of chemisorption have been used to calculate the activation energies and heats of surface reactions at 300 K using UBI-QEP. These properties were assumed to be temperature independent. Table 1 shows the results of thermodynamic consistency tests done at 1450 K, the average temperature of the LIF experiments against which the mechanism was optimized. Even though the mechanism is enthalpically consistent at 300 K (because all energetic parameters were estimated using the gaseous-species database at 300 K), it gives considerable errors at high temperatures, as shown in Table 1. Note that although the difference of the equilibrium constants of the gas-phase reaction and its corresponding surface reaction is well within a factor of 4, this relatively small difference results from cancellation of errors in individual K^{eqH} and K^{eqS} of the reactions steps involved. The errors are significant for other reaction cycles, such as the dissociation of H_2, O_2, and H_2O.

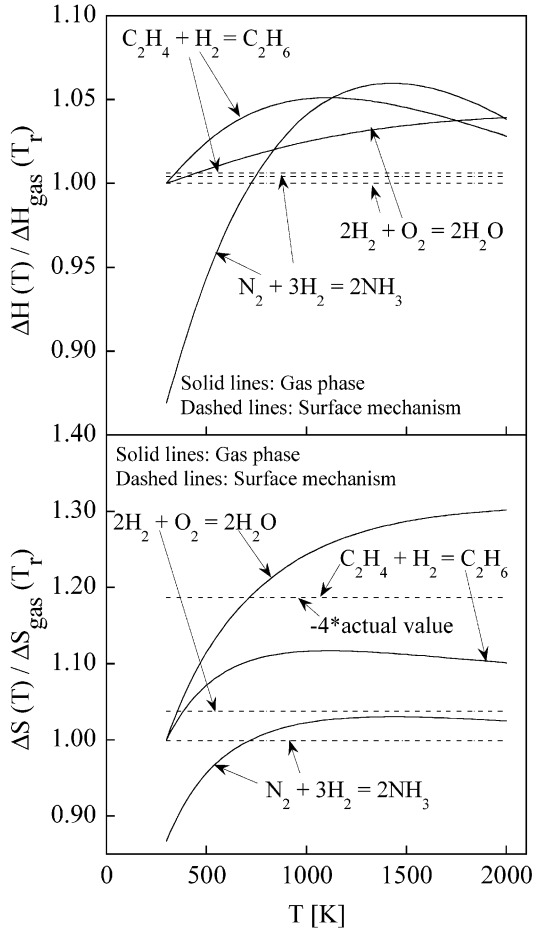

Figure 1. Normalized enthalpy and entropy of overall gas-phase reactions versus temperature for three reactions indicated using the GRI 3.0 thermodynamic database[61] and values from the surface reaction mechanisms of Rekoske et al.,[30] Stoltze and Norskov,[46−49] and Aghalayam et al.[21] The normalization is done with respect to the corresponding gas-phase quantity at a reference temperature T_r. Note that in the bottom panel, the curve corresponding to the mechanism of Rekoske et al. has been multiplied by −4. The reference temperature T_r is 300, 723, and 300 K, for ethylene hydrogenation, ammonia synthesis, and hydrogen oxidation, respectively.

The reaction mechanism just discussed has 9 reversible reactions ($I = 9$), a total of 10 species ($K = 10$), and 4 surface species ($K_s = L = 4$). The number of degrees of freedom equals $I - L = 5$. Therefore, parameter adjustment in this case is not as trivial as those of the previous examples. In a later section, we shall discuss our approach toward thermodynamic consistency, using the same mechanism as our test case.

Effect of Temperature. Most surface reaction mechanisms developed so far are at best thermodynamically consistent at a single temperature. However, operation from start up to normal operating conditions and eventually to shut down demands variations in temperature. These variations could be as large as several hundred degrees. Currently, there is no systematic approach to ensure thermodynamic consistency of surface reaction mechanisms as temperature varies. Here we present a few examples to assess how reaction mechanisms perform thermodynamically as a function of temperature.

Figure 1 shows the variation of enthalpy and entropy as a function of temperature for the reactions presented in Table 1 and discussed in the previous sections. In these plots, the enthalpy and entropy values are normalized by their respective values calculated from the gas-phase thermochemical data at a reference temperature, T_r. The solid lines denote the enthalpy and entropy based entirely on gas-phase thermochemical data, and the dashed lines represent those implied by the surface reaction mechanism as they are computed from the prefactors and activation energies using eqs 10b and 11b. Thermodynamic inconsistency is reflected by the deviation between the solid and dashed lines for a given reaction. Clearly, none of mechanisms is thermodynamically consistent over an extended temperature range. It should be noted that the Stoltze and Norskov used rigorous temperature dependence through partition functions; however, we have used the mechanism from the paper of Dumesic and Trevino just to illustrate the importance of temperature effects.

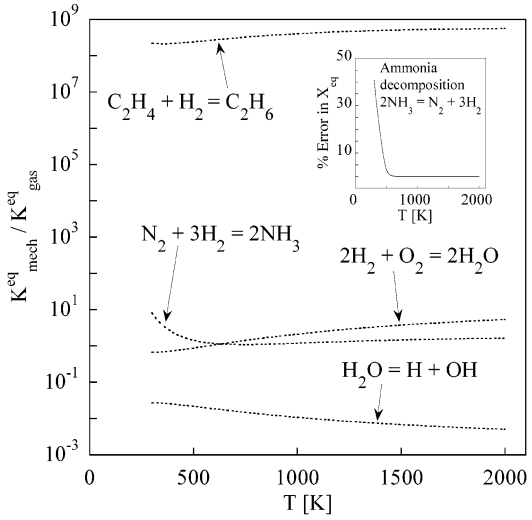

Figure 2. Equilibrium constant of a surface reaction cycle over the corresponding overall gas-phase reaction versus temperature. The gas-phase calculations are performed using the GRI 3.0 thermodynamic database.[61] The mechanisms are unable to handle the effect of temperature on the equilibrium constants. The inset shows the percentage error in the equilibrium conversion (X_{eq}) of ammonia decomposition ($2NH_3 \leftrightarrow N_2 + 3H_2$ at 1 atm) when the equilibrium constant is calculated from the surface reaction mechanism.

Figure 2 shows the equilibrium constants of the reactions of Table 1 given by the surface reaction rate parameters normalized by the equilibrium constants determined by the more accurate gas-phase thermochemistry. Thus, the ratio of equilibrium constants is unity or close to unity if a reaction mechanism is thermodynamically consistent. It is seen that the equilibrium constants for ethylene hydrogenation differ by 8 orders of magnitude. The equilibrium constant for the H_2 oxidation reaction cycle matches well with the corresponding gas-phase equilibrium constant, although this is a result of cancellation of errors. This is illustrated using a different reaction cycle of water decomposition in the H_2 oxidation mechanism in Figure 2 where the equilibrium constants differ by 2 orders of magnitude.

It is well-known that the enthalpies and entropies of the overall gaseous reactions depend slightly on temperature, with a maximum deviation of 25−30% over the considered temperature range (see also Figure 1). As a result, over the range 300−2000 K, the ratio of the equilibrium constants changes by a factor of approximately 2.5, 5, 8, and 5.5 for ethylene hydrogenation, ammonia synthesis, hydrogen oxidation, and water decomposition reactions, respectively (see Figure 2). The inset in Figure 2 shows the percentage error in the equilibrium conversion (X_{eq}) for ammonia decomposition ($2NH_3 \leftrightarrow N_2 +$

$3H_2$ at 1 atm) when equilibrium constants calculated from the mechanism are used instead of those calculated using the gas-phase database. Errors as high as 41% are observed in the equilibrium conversion at low temperatures, where the equilibrium constants of the gas phase and the surface mechanism differ by a factor of 8.2 for this reaction. The errors in equilibrium conversion can be much larger for other reactions. The significant errors in the equilibrium constants and the equilibrium conversion indicate the need for ensuring thermodynamic consistency as a function of temperature when temperature varies over a wide range.

Semiempirical or Quantum Chemical Methods and Thermodynamic Consistency

Here we discuss how semiempirical and DFT methods could be interfaced with parameter estimation while thermodynamic consistency is ensured at the enthalpic level. Entropic consistency may be ensured using TST and statistical mechanics formulas.

Bond Order Conservation. UBI-QEP is a practical tool when a large number of surface reactions need to be considered in the mechanism. Examples of this approach include our development of surface reaction mechanisms for H_2 oxidation on Pt,[21] CO oxidation on Pt,[22] and CH_4 oxidation on Pt.[23,24] Heats of chemisorption are estimated using the UBI-QEP method and used as independent parameters. Then the heats of reactions (dependent parameters) are calculated using eq 10a. Activation energies are computed within the UBI-QEP framework as a function of heats of chemisorption and satisfy eq 10b. Thus, enthalpic consistency is naturally satisfied on both a single reaction level and any overall reaction level.

Polanyi Free Energy Relations. Polanyi free energy relations are commonly used in complex reaction networks.[41,51,52] The activation energy of the ith reaction is a sum of the intrinsic barrier, E_i^*, characteristic of the homologous series and a fraction of the heat of reaction

$$E_i = E_i^* + \alpha_i \Delta H_i \tag{12}$$

where α_i is known as the transfer coefficient. By choosing L reaction steps (e.g., adsorption/desorption steps) as the basis, the heats of all other reactions can be computed using eq 10a. Consequently, eq 12 can be employed to estimate activation energies of all reactions well within the framework of thermodynamic consistency advocated herein.

First Principles Techniques: Density Functional Theory. The critical geometry corresponding to a transition state and the critical energy can be directly estimated by ab initio methods. This approach has a specific advantage that the rate parameters would be thermodynamically consistent, given that there is no additional input from any other source. Though these methods are attractive, they are unfortunately not always accurate at the current level of theory and computational capability. It is known that the DFT vibrational frequencies and critical energy are associated with errors that could result in an uncertainty factor from a few factors to over an order of magnitude in the predicted rate constant. For this reason, some tuning or optimization of the rate parameters is inevitable if one is interested in a predictive reaction mechanism. As discussed in the Introduction, in addition to the DFT errors, the nonideality of the real catalytic surface often requires the rate parameters be tuned to predict a specific set of experiments. We approach optimization, by imposing the thermodynamic constraints, as discussed below.

Optimization Strategies

The quantitative relations given by eqs 10b and 11b can be used in *rate parameter optimization* as *implicit* constraints in the least-squares objective function,

$$f = w_y \sum_{n=1}^{N} (Y_n^{exp} - Y_n^{model})^2 + w_e \sum_{n=1}^{N'} \sum_{i=L+1}^{I} [E_{i,n}^f - E_{i,n}^b - \sum_{j=1}^{L} c_{ij} \times$$

$$(E_j^f - E_j^b)]^2 + w_a \sum_{n=1}^{N'} \sum_{i=L+1}^{I} [\ln(A_{i,n}^f/A_{i,n}^b) - \ln \prod_{j=1}^{L} (A_j^f/A_j^b)^{c_{ij}}]^2 \tag{13}$$

Here the first term gives the difference between model predictions and target experimental data and the last two impose thermodynamic constraints on the reaction rate parameters, N is the number of experimental points considered in the optimization, N' is the number of (temperature) points where entropic and enthalpic consistency is imposed, Y^{model} is the model response, Y^{exp} is the corresponding experimental data, and w_y, w_e, and w_a are the weights.

Alternatively, the constraints can be *explicitly* placed on the rate parameters that go into the computation of Y^{model} by using the algebraic constraints eqs 10b and 11b and setting $w_e = w_a = 0$. Although this approach appears to be more rigorous, it may lead to an overconstrained system and poor fitting of experimental data. Furthermore, because there is an uncertainty associated with thermodynamic databases, enforcing consistency through algebraic constraints may be too demanding, as will be demonstrated later.

As the heats of chemisorption and activation energies are generally more readily available than the prefactors, for demonstration purposes we choose to keep activation energies fixed and optimize the prefactors only. Optimization of the prefactors is carried out subject to constraints, which ensure entropic consistency. For implicit thermodynamic constraints, we choose the joint objective function in the form of

$$f = w_y \sum_{n=1}^{N} (1 - Y_n^{model}/Y_n^{exp})^2 +$$

$$w_a \sum_{n=1}^{N'} \sum_{i=L+1}^{I} \left(1 - \frac{\ln[(A_{i,n}^f/A_{i,n}^b)/\prod_{j=1}^{L} (A_{j,n}^f/A_{j,n}^b)^{c_{ij}}]}{\Delta S_{i,n}^{gas}} \right)^2 \tag{14}$$

In comparison to eq 13, normalization is introduced and the weights are therefore chosen to be unity, $w_y = w_a = 1$. To account for the temperature effect, the entropy constraint (the second term in eq 14) is imposed over the range of temperature defined by experiments. When the range of temperature is narrow or for isothermal systems, one can extend the range around the temperature of interest. In that case, we have $N' > N$.

We choose to demonstrate mechanism optimization with thermodynamic constrains for a specific example of surface reaction mechanism of H_2 oxidation on Pt.[21] The optimization target is the low-pressure LIF experiments on a polycrystalline Pt foil.[53] Thus, optimization is carried out with $N = 18$ experimental data points over the temperature range 1100−1800 K. Eighteen temperature values ($N' = 18$) are selected, covering the temperature range 300−2000 K. The reactor is modeled as a steady-state continuously stirred tank reactor due to the low pressure and thus the large mean free path.

TABLE 2: Surface Reaction Mechanisms for H_2 Oxidation on Pt[a]

no.	reaction	initial prefactor A	optimized prefactor A or A_o	temperature exponent β	activation energy E^b
S_1	$H_2 + 2* \rightarrow 2H*$		0.042	0	0
		1	0.034	0.675	
			0.127	0.955	
S_2	$2H* \rightarrow H_2 + 2*$		4.04×10^{14}	0	$17.9-6.0\theta_H$
		1×10^{13}	1.84×10^{14}	−0.840	
			5.57×10^{13}	−0.955	
S_3	$O_2 + 2* \rightarrow 2O*$		0.994	0	0
		0.1	0.191	−0.015	
			0.684	0.267	
S_4	$2O* \rightarrow O_2 + 2*$		1.01×10^{12}	0	$51-32\theta_o$
		1×10^{13}	3.28×10^{12}	−0.109	
			7.92×10^{12}	−1.266	
S_5	$OH* + * \rightarrow H* + O*$		2.19×10^{11}	0	$27.3 - f(\theta)$
		1×10^{11}	3.36×10^{11}	0.280	
			6.11×10^{11}	0.696	
S_6	$H* + O* \rightarrow OH* + *$		2.20×10^{10}	0	$8.2 - f(\theta)$
		1×10^{11}	9.72×10^{9}	−0.565	
			1.64×10^{10}	−0.696	
S_7	$H_2O* + * \rightarrow H* + OH*$		9.72×10^{12}	0	$18.1 - f(\theta)$
		1×10^{11}	2.81×10^{11}	1.966	
			1.17×10^{11}	0.765	
S_8	$H* + OH* \rightarrow H_2O* + *$		8.99×10^{11}	0	$12.9 - f(\theta)$
		1×10^{11}	6.35×10^{10}	1.894	
			8.57×10^{10}	−0.765	
S_9	$H_2O* + O* \rightarrow 2OH*$		1.14×10^{9}	0	$8.8 - f(\theta)$
		1×10^{11}	1.23×10^{9}	−1.496	
			1.91×10^{10}	0.069	
S_{10}	$2OH* \rightarrow H_2O* + O*$		1.06×10^{9}	0	$22.7 - f(\theta)$
		1×10^{11}	9.63×10^{9}	−0.719	
			5.23×10^{11}	−0.069	
S_{11}	$OH + * \rightarrow OH*$		0.031	0	0
		1	0.014	−0.258	
			0.043	0.250	
S_{12}	$OH* \rightarrow OH + *$		1.29×10^{14}	0	$63-33\theta_o$
		1×10^{13}	6.75×10^{14}	−0.342	
			5.23×10^{14}	−0.250	
S_{13}	$H_2O + * \rightarrow H_2O*$		0.015	0	0
		0.7	0.012	1.966	
			0.051	0.250	
S_{14}	$H_2O* \rightarrow H_2O + *$		9.01×10^{14}	0	10
		1×10^{13}	4.47×10^{15}	0.652	
			4.39×10^{14}	−0.250	
S_{15}	$H + * \rightarrow H*$		0.152	0	0
		1	0.349	−0.569	
			0.086	0.250	
S_{16}	$H* \rightarrow H + *$		3.48×10^{14}	0	$61-3\theta_H$
		1×10^{13}	3.74×10^{14}	−0.876	
			2.61×10^{13}	−0.250	
S_{17}	$O + * \rightarrow O*$		0.006	0	0
		1	0.082	−1.563	
			0.172	0.250	
S_{18}	$O* \rightarrow O + *$		1.99×10^{11}	0	$85-16\theta_o$
		1×10^{13}	7.75×10^{12}	−1.298	
			1.30×10^{13}	−0.250	

[a] Sticking coefficients are unitless, preexponentials in s^{-1}, and activation energies in kcal/mol. The coverage dependence of the desorption energy is linear, whereas that of Langmuir−Hinshelwood surface reactions (f is nonlinear) is given through the UBI-QEP formulas. For the screening mechanism, all temperature exponents β are equal to zero and the activation energies are constant. In the optimized prefactor column, the first, second, and third entry for each reaction corresponds to cases a, b, and c, respectively (see text). In case c, the A_o value is reported. The reference temperature is $T_o = 300$ K. The activation energies in the table are at the reference temperature. [b] The variation of the activation energies as a function of temperature is considered (see text).

The screening surface reaction mechanism is presented in Table 2 and consists of 18 irreversible reactions ($I = 9$ reversible steps) and $K_s = L = 4$ species. In this mechanism, the prefactors are initially estimated from TST, on the basis of the type of reaction[2] (e.g., 10^{13} s^{-1} for desorption steps and 10^{11} s^{-1} for Langmuir−Hinshelwood bimolecular reaction). The activation energies given in Table 2 are obtained from UBI-QEP and thermodynamically consistent at 300 K. The variation of the reaction enthalpy and hence the activation energies vs temperature are considered using statistical mechanical formulas developed in Appendix B. The resulting variations of heats of chemisorption as a function of temperature are summarized in Table 3. In all cases, these variations are of the order of $R\Delta T$ and thus represent small corrections to the heats of chemisorption (except for extremely weakly bound species such as H_2O*).

Under the UBI-QEP framework, these temperature dependent heats of chemisorption lead to temperature-dependent activation energies and heats of surface reactions. Activation energies of

TABLE 3: Variation of Heats of Chemisorption (ΔQ) as a Function of Temperature (See Appendix B for Details)[a]

type of reaction	ΔQ
monatomic adsorption, e.g., H + * → H*	$^3/_2 R\Delta T$
diatomic adsorption, e.g., OH + * → OH*	$2R\Delta T$
nonlinear polyatomic adsorption, e.g., H_2O + * → H_2O*	$^5/_2 R\Delta T$

[a] R is the universal gas constant, and $\Delta T = T - T_o$, the temperature difference from a reference temperature T_o at which the original heats of chemisorption values are calculated/measured.

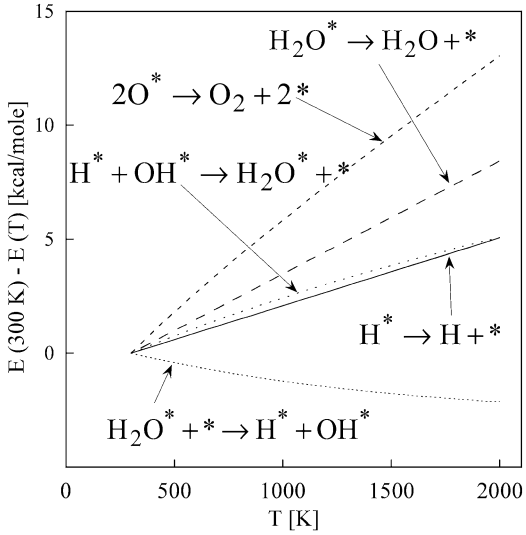

Figure 3. Deviation of temperature-dependent activation energies from their values at 300 K for selected reaction steps in the H_2 oxidation mechanism on Pt. Statistical mechanical formulas are employed (see Table 3 and Appendix B) for calculation of temperature dependent heats of chemisorption and the UBI-QEP framework for computing the activation energies. The temperature variation of activation energies is almost linear and is small for Langmuir−Hinshelwood surface reactions but larger for weakly adsorbed species.

selected reactions are shown in Figure 3 as a function of temperature. Over the temperature range 300−2000 K, the variation in the activation energy is largest for the desorption of polyatomic molecules, and within ∼5−6 kcal/mol for the Langmuir−Hinshelwood type surface reactions. The decrease in activation barriers with increasing temperature was also observed earlier by Hansen and Neurock for ethylene hydrogenation on Pd.[9] We have implemented statistical mechanical formulas in the UBI-QEP framework in Surface CHEMKIN[54] format.

Figure 4 shows the comparison of the experimental data (symbols) and predictions with the screening mechanism (solid line). Obviously, the reaction mechanism does not predict the experimental data well, although the basic experimental trend is well captured by the model.

In our analysis of thermodynamic consistency of the reaction mechanism (Table 2), the reversible adsorption/desorption reaction steps, S_{11} through S_{18}, are taken as the basis set. This leaves $I - L = 5$ reversible reaction cycles (S_1 through S_{10}), which include 3 Langmuir−Hinshelwood type surface reactions (S_5 through S_{10}) and the adsorption/desorption steps of H_2 and O_2 (S_1 through S_4).

Minimization of eq 14 is carried out using the IMSL subroutine zxmwd.[55] For the present purpose, we solved Y^{model} by direct solution of the underlying governing equations, without invoking the response surface methodology.[56] During optimization, physical bounds are considered for prefactors depending on the type of reaction,[57,58] as listed in Table 4. By putting such large bounds, enough flexibility is allowed in the optimization, whereas the prefactors remain physically acceptable. Three cases of varying complexity in the temperature dependence of the prefactors were considered. These cases are discussed below.

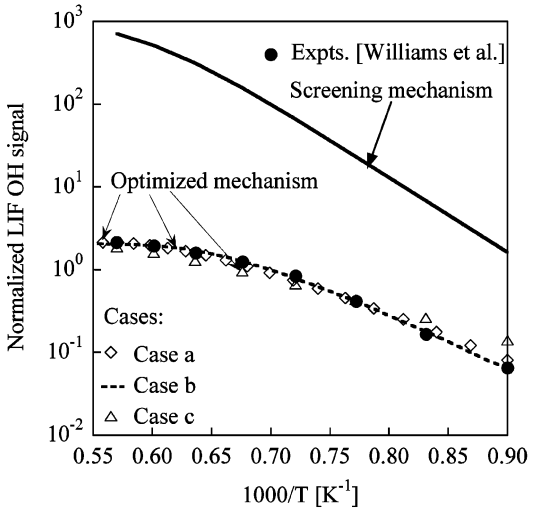

Figure 4. Prediction of the screening H_2 oxidation mechanism on polycrystalline Pt against the experimental LIF data of Williams et al.[53] (solid line). Predictions using three sets of optimized parameters of the H_2/O_2/Pt mechanism against the experimental data of Williams et al.[53] are also shown. Case a: optimization with temperature independent prefactors (except for adsorption). Case b: optimization with temperature-dependent prefactors using the objective function eq 14. Case c: optimization with temperature dependent prefactors using algebraic constraints. The mechanism captures well experimental data, while being thermodynamically consistent at all temperatures.

TABLE 4: Typical Ranges of Prefactors of Surface Reactions Estimated Using TST[a,57,58]

type of reaction	prefactor range[b]
adsorption (H + * → H*)	5×10^{-3} to 1
atomic desorption (O* → O + *)	10^{11} to 10^{16}
molecular desorption (OH* → OH + *)	10^{13} to 10^{16}
associative desorption (2H* → H_2 + 2*)	10^{12} to 10^{16}
Langmuir−Hinshelwood reaction (H_2O* + * → H* + OH*)	10^9 to 10^{13}

[a] For each type of reaction, an example from the H_2 oxidation mechanism is shown. [b] The sticking coefficients are unitless, and the unit of the reaction prefactors is s^{-1}.

Implicit Thermodynamic Constraints: Simple Arrhenius Equation (Case a). In case a, the prefactors are assumed to be independent of temperature (except for sticking coefficients which vary with temperature as described by kinetic theory for the collision flux). The optimized prefactors are shown in Table 2. The optimized mechanism is able to capture well the experimental data, as seen in Figure 4. At the same time, the optimized mechanism gives drastically improved entropic consistency over the trial mechanism, as seen in Figure 5 (dashed lines). The equilibrium constant of all reaction cycles matches that of the corresponding gas phase reaction to within a factor of 4.6 over the entire temperature range. The cause for this discrepancy is obvious, in that the temperature variation of entropy, or its subsequent effect on the prefactors is not rigorously captured here. The fundamental limitation lies in the use of a simple Arrhenius equation to describe the reaction rate

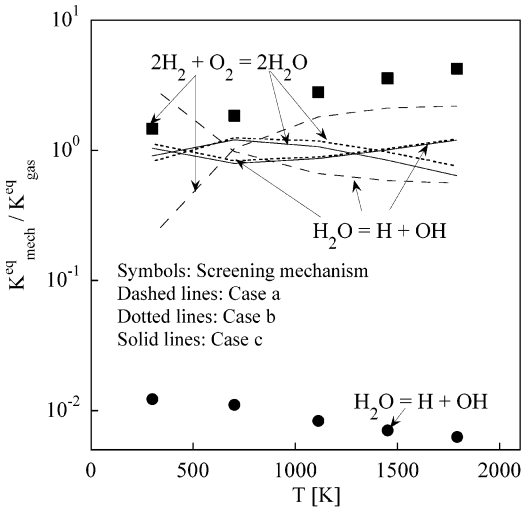

Figure 5. Ratio of the equilibrium constants of the surface reaction mechanism over the gas-phase one versus temperature for two selected examples, the overall reaction of H_2 oxidation and water decomposition (the entire mechanism is also thermodynamically consistent). Symbols correspond to the screening mechanism, dashed lines to the optimized mechanism of case a, dotted lines to the optimized mechanism of case b, and solid lines to the optimized mechanism of case c. The screening mechanism is thermodynamically inconsistent. The equilibrium constants of the optimized mechanisms match well the corresponding gas-phase ones over the entire temperature range.

constant and can be removed by using the modified Arrhenius equation as described in case (b).

Implicit Thermodynamic Constraints: Modified Arrhenius Equation (Case b). To rigorously account for the temperature variation in entropic consistency, we propose to use the modified Arrhenius expression

$$k = A\left(\frac{T}{T_0}\right)^{\beta} \exp\left(-\frac{E}{RT}\right) \tag{15}$$

where T_0 is the reference temperature, $T_0 = 300$ K, and b is the temperature exponent. In this case, a total of 36 optimization parameters (18 prefactors and 18 temperature exponents) are considered in the optimization procedure.

The optimized parameters are shown in Table 2. The optimized mechanism captures well experimental data, as seen in Figure 4. Figure 5 shows the resulting equilibrium constants of the overall H_2 oxidation and water decomposition reactions over their gaseous counterparts (dotted lines). These equilibrium constants are now within 24.2% from the corresponding gas-phase equilibrium constants, compared to a factor of 4.6 found in case a. Thus, a significant improvement is apparent in thermodynamic consistency.

Explicit Thermodynamic Constraints: Modified Arrhenius Equation (Case c). We proceed as in case b, using the optimization eq 14, but here we select the entropies of the adsorption/desorption steps ($S_{11}-S_{18}$) as the independent variables (we set $w_a = 0$). During the optimization process, the ratios of prefactors of the remaining 5 reaction steps (S_1-S_{10}) are calculated using explicit, algebraic constraints, eq 11b, at 8 selected temperatures in the range 300−2000 K. This ratio is then equally distributed in the forward and backward prefactor such that the overall ratio satisfies the algebraic constraint. If the estimated sticking coefficient of any step exceeds 1.0, it is forced to 1.0 and the corresponding backward prefactor is properly adjusted. These temperature-dependent prefactors are then fitted using the following power law equation

$$A = A_0\left(\frac{T}{T_0}\right)^{\beta} \tag{16}$$

The values of A_0 and temperature exponents are passed to the model to generate the model response Y_i^{model}, at each experimental point i.

In the objective function, 8 experimental data are selected in the range 1100−1800 K. The optimized parameters are presented in Table 2 and the mechanism performance is presented in Figure 4. The equilibrium constants are shown in Figure 5 (solid lines). These equilibrium constants are now within 36.3% from the corresponding gas-phase equilibrium constants. The error arises from the temperature variation of prefactors described by eq 16. The mechanism captures experimental data well and is thermodynamically consistent over the entire temperature range considered.

A comparison of least-squares residuals, with respect to the experimental data only, shows that case b captures the experimental data more accurately (residual $= 8 \times 10^{-6}$) than case a (residual $= 3 \times 10^{-5}$), and case c is the worst (residual $= 4 \times 10^{-4}$). The decreased accuracy in the explicit approach of case c is due to the highly constrained system, whereas the improved accuracy in case b is due to the flexibility through a large number of optimization parameters. Nonetheless, both cases b and c are acceptable with regard to accuracy in predicting the experimental data, and the excellent thermodynamic consistency of the optimized mechanisms.

We performed a sensitivity analysis on the optimized, but entropically inconsistent, surface reaction mechanism of ref 59 (denoted as II) and the optimized mechanism of case c (denoted as I). Figure 6 shows the sensitivity spectra. It is observed that the relative importance of influential reaction steps is similar in the two mechanisms. At low temperatures (panel a), adsorption−desorption steps play a significant role, whereas at high temperatures (panel b), Langmuir−Hinshelwood surface reactions are somewhat important.

Finally, due to the different number of unknowns involved in the optimization, the CPU time varies considerably between the three cases. In particular, it is about 2 days for case a, 4 days for case b, and 12 h for case c, on a Pentium IV 1.9 GHz Dell processor.

Conclusions

In this paper we reviewed criteria of thermodynamic consistency of an entire reaction mechanism. We then derived criteria when adsorption/desorption steps constitute the basis of a surface reaction mechanism and assessed the thermodynamic consistency of selected published mechanisms. Apart from computationally intensive DFT calculations, semiempirical techniques, such as UBI-QEP and Polanyi free energy relations, can be combined with optimization to tackle the thermodynamic consistency of surface reaction mechanisms. Various optimization approaches were discussed and applied to a specific example of surface reaction mechanism for H_2 oxidation on Pt. We have shown that temperature effects are important to capture thermodynamic consistency, and modified Arrhenius prefactors are suitable to achieve this task. Optimization based on algebraic constraints has the advantage of reducing the number of unknowns, and the CPU requirements but may result in slightly worse prediction of experimental data by overconstraining the system and propagating the uncertainty of thermodynamic

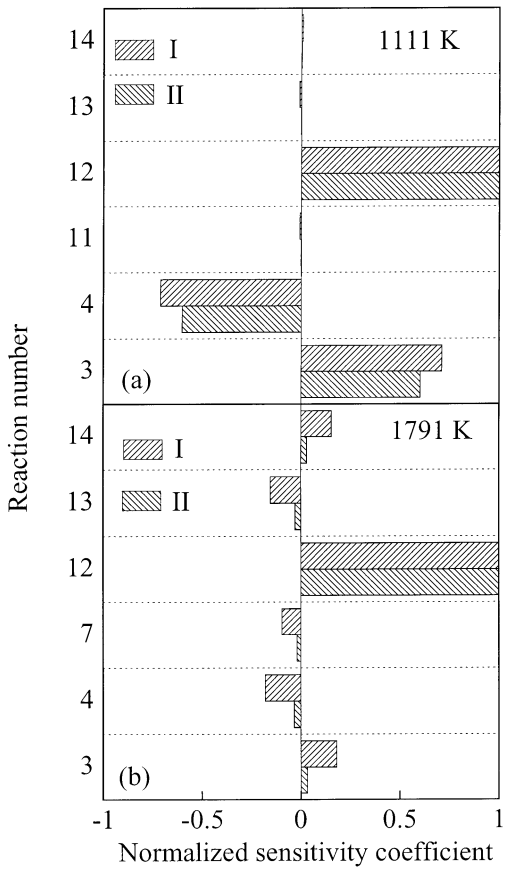

Figure 6. Comparison of sensitivity analysis of an optimized mechanism without thermodynamic consistency constraints (II), taken from ref 59, with that of the optimized, thermodynamically consistent mechanism of case c (I). Panels a and b correspond to low and high temperatures, respectively. The overall sensitivity features are similar for both mechanisms with Langmuir−Hinshelwood surface reactions becoming slightly important at high temperature. The reaction numbers on the vertical axes correspond to Table 2.

database in the kinetic parameters. Overall, this approach can contribute to the development of making surface reaction rate parameters realistic and thermodynamically consistent.

Acknowledgment. This work was prepared with the support of the U.S. Department of Energy, under Award no. DE-FC26-00NT41027 and the Army Research Office under contract DAAD19-01-1-0582. However, any opinions, findings, conclusions, or recommendations expressed herein are those of the authors and do not necessarily reflect the views of the DOE or the Army Research Office.

Appendix A: Row Echelon Reduction for Mechanism Analysis

A matrix is in reduced row Echelon form if it has the following properties:

1. The first nonzero element in any nonzero row is "1".
2. The leading "1" in any nonzero row belongs to a column, whose every other element is zero.
3. Each such leading "1" appears after every preceding row's leading "0"'s.

The reduced row Echelon form of a matrix helps to calculate the degrees of freedom for the system of equations constituting the matrix, or in other words, it helps to calculate the rank of the matrix. In this paper, this idea is employed to identify the linearly independent and dependent reactions in a mechanism.

A matrix **P** of stoichiometric coefficients of the reactions is created in such a way that

1. Reactants have negative stoichiometric coefficients.
2. Products have positive stoichiometric coefficients.
3. The rows of the matrix correspond to the species in the mechanism.
4. The columns of the matrix correspond to the reactions in the mechanism.

These calculations are very easy to perform in Matlab. For example, the Matlab command rank (A) gives the rank of matrix **A**. The Matlab command [R,V] = rref[A] gives the reduced row Echelon form of matrix **A** saved in matrix **R**, and the vector **V** represents the linearly independent reactions. The dimension of the vector **V** corresponds to the number of linearly independent reactions and its entries show which reactions are linearly independent and form a basis. The columns of **R** corresponding to linearly dependent reactions show the coefficients of decomposing these dependent reactions to the basis according to eq 6.

As an example, consider the following three reactions with four species H*, O*, OH*, and H_2O*

$$H^* + O^* = OH^* + * \quad \text{(R1)}$$

$$H^* + OH^* = H_2O^* + * \quad \text{(R2)}$$

$$2OH^* = H_2O^* + O^* \quad \text{(R3)}$$

Vacancies are not considered as a surface species. The matrix **A**

$$\mathbf{A} = \begin{bmatrix} -1 & -1 & 0 \\ -1 & 0 & 1 \\ 1 & -1 & -2 \\ 0 & 1 & 1 \end{bmatrix} \begin{matrix} H^* \\ O^* \\ OH^* \\ H_2O^* \end{matrix}$$

is input as **A** = [−1 −1 0; −1 0 1; 1 −1 −2; 0 1 1] and its reduced row Echelon form **R** is computed using Matlab

$$\mathbf{R} = \begin{bmatrix} 1 & 0 & -1 \\ 0 & 1 & 1 \\ 0 & 0 & 0 \\ 0 & 0 & 0 \end{bmatrix}$$

The vector **V** = [1 2] indicates that reactions 1 and 2 are linearly independent (in this case direct calculation shows that the rank of **A** is 2). In fact, the third reaction R3 can be obtained as a linear combination of reactions R1 and R2 using the last column of the matrix **R** as R3 = −R1 + R2.

Appendix B: Heats of Chemisorption

The enthalpy of reaction at an arbitrary temperature $\Delta H(T)$ is related to the enthalpy of reaction at 0 K, $\Delta H(0)$, and the sensible heat of the reactants and products by

$$\Delta H(T) = \Delta H(0) + \int_0^T \mathrm{d}H_{\text{products}} - \int_0^T \mathrm{d}H_{\text{reactants}}$$

where the last two terms represent the sensible heats, which are readily available for simple adsorption reactions of types discussed below.

Adsorption of Monatomic Molecule, e.g., H + * → H* and O + * → O*. Upon adsorption, a monatomic gas molecule converts its three translational degrees of freedom to three

vibrational degrees of freedom. If we assume that the vibrational frequencies associated with the surface species are identical (ν_{vs}) and harmonic, the partition function of each degree of freedom is $\exp(kT/2h\nu_{vs})/[\exp(kT/h\nu_{vs}) - 1]$, which at the high-temperature limit is $kT/(h\nu_{vs})$, where k is the Boltzmann constant and h is the Planck constant.[60] For typical ν_{vs} values, the partition function at the high-temperature limit is sufficiently accurate for temperature above 300 K. We note that more accurate vibrational frequencies can be obtained from DFT or experiments, if higher accuracy is required.

The loss and gain in different types of degrees of freedom contribute toward sensible heat. In particular,

loss due to three translational degrees of freedom = $3RT/2$

gain due to three vibrational degrees of freedom = $3RT$

Therefore, the enthalpy of reaction at an arbitrary temperature is

$$\Delta H(T) = \Delta H(0) + \frac{3}{2}RT$$

where R is the universal gas constant. Because ΔH is typically a negative quantity for adsorption, the heat of adsorption decreases with increasing temperature, as expected.

Adsorption of Diatomic Molecule, e.g., OH + * → OH*. Upon adsorption, a diatomic gas molecule converts its three translational and two rotational degrees of freedom into five vibrational degrees of freedom on the surface, among which one vibrational degree of freedom can be approximated as a free, internal rotor (i.e., rotation of the H about the principal axis defined by the O−Pt bond). The vibrational frequency of the diatomic stretch motion is assumed to be the same before and after surface adsorption. Employing the high-temperature limit assumption as in the monatomic case, we have

loss due to three translational degrees of freedom = $3RT/2$

loss due to two rotational degrees of freedom = RT

gain due to four vibrational degrees of freedom = $4RT$

gain due to one rigid rotor type degree of freedom = $RT/2$

Therefore, the enthalpy of reaction at an arbitrary temperature is

$$\Delta H(T) = \Delta H(0) + 2RT$$

Adsorption of Nonlinear Polyatomic Molecule, e.g., H_2O + * → H_2O*. Upon adsorption, the triatomic H_2O molecule converts its three translational and three rotational into six vibrational degrees of freedom on the surface, among which one vibrational degree of freedom can be approximated as a free, internal rotor (i.e., rotation of the H−O−H group about the principal axis defined by the O−Pt bond). The vibrational frequencies of the stretching and bending motion are assumed to be the same before and after surface adsorption. Using the high-temperature limit assumption, we found that

loss due to three translational degrees of freedom = $3RT/2$

loss due to three rotational degrees of freedom = $3RT/2$

gain due to five vibrational degrees of freedom = $5RT$

gain due to one rigid rotor type degree of freedom = $RT/2$

Therefore, the enthalpy of reaction at an arbitrary temperature is

$$\Delta H(T) = \Delta H(0) + \frac{5}{2}RT$$

The formulas of relevance to the current work are compiled in Table 3.

References and Notes

(1) Bush, S. F.; Dyer, P. *Proc. R. Soc. London A* **1976**, *351*, 33.
(2) Dumesic, J. A.; Rudd, D. F.; Aparicio, L. M.; Rekoske, J. E.; Trevino, A. A. *The Microkinetics of Heterogeneous Catalysis*; American Chemical Society: Washington, DC, 1993.
(3) Stoltze, P. *Prog. Surf. Sci.* **2000**, *65*, 65.
(4) Broadbelt, L. J.; Snurr, R. Q. *Appl. Catal. A: Gen.* **2000**, *200*, 23.
(5) Raimondeau, S.; Vlachos, D. G. *Chem. Eng. Sci.* **2003**, *58*, 658.
(6) Raimondeau, S.; Vlachos, D. G. *Comput. Chem. Eng.* **2002**, *26*, 965.
(7) Volkening, S.; Wintterlin, J. *J. Chem. Phys.* **2001**, *114*, 6382.
(8) Raimondeau, S.; Aghalayam, P.; Vlachos, D. G.; Katsoulakis, M. Bridging the gap of multiple scales: From microscopic, to mesoscopic, to macroscopic models. Foundations of Molecular Modeling and Simulation, 2000, Colorado.
(9) Hansen, E. W.; Neurock, M. *J. Catal.* **2000**, *196*, 241.
(10) Yang, W.-S.; Xiang, H.-W.; Li, Y.-W.; Sun, Y.-H. *Catal. Today* **2000**, *61*, 237.
(11) van Santen, R. A.; Neurock, M. *Catal. Rev.−Sci. Eng.* **1995**, *37*, 557.
(12) Norskov, J. K. *Stud. Surf. Sci. Catal.* **1999**, *122*, 3.
(13) Lund, C. R. F. *Ind. Eng. Chem. Res.* **1996**, *35*, 2531.
(14) Waugh, K. C. *Catal. Today* **1999**, *53*, 161.
(15) Shustorovich, E. *Adv. Catal.* **1990**, *37*, 101.
(16) Shustorovich, E.; Sellers, H. *Surf. Sci. Rep.* **1998**, *31*, 1.
(17) Bronsted, N. *Chem. Rev.* **1928**, *5*, 231.
(18) Evans, M. G.; Polanyi, M. *Trans. Faraday Soc.* **1938**, *34*, 11.
(19) Hei, M. J.; Chen, H. B.; Yi, J.; Lin, Y. J.; Lin, Y. Z.; Wei, G.; Liao, D. W. *Surf. Sci.* **1998**, *417*, 82.
(20) Fishtik, I.; Datta, R. *Surf. Sci.* **2002**, *512*, 229.
(21) Aghalayam, P.; Park, Y. K.; Vlachos, D. G. *AIChE J.* **2000**, *46*, 2017.
(22) Aghalayam, P.; Park, Y. K.; Vlachos, D. G. *Proc. Combust. Inst.* **2000**, *28*, 1331.
(23) Aghalayam, P.; Park, Y. K.; Fernandes, N. E.; Papavassiliou, V.; Mhadeshwar, A. B.; Vlachos, D. G. *J. Catal.* **2003**, *213*, 23.
(24) Mhadeshwar, A. B.; Aghalayam, P.; Papavassiliou, V.; Vlachos, D. G. *Proc. Combust. Inst.* **2003**, *29*, 997.
(25) Raimondeau, S.; Vlachos, D. G. *Chem. Eng. J.* **2002**, *90*, 3.
(26) Mhadeshwar, A. B.; Kragten, D. D.; Vlachos, D. G. *Joint Mtg. U.S. Sect. Combust. Inst., 3rd* **2003**, Paper No. E2.
(27) Ishikawa, Y.; Liao, M.; Cabrera, C. R. *Surf. Sci.* **2000**, *463*, 66.
(28) Ovesen, C. V.; Clausen, B. S.; Hammershoi, B. S.; Steffensen, G.; Askguard, T.; Chorkendorff, I.; Norskov, J. K.; Ragmussen, P. B.; Stolze, P.; Taylor, P. *J. Catal.* **1996**, *158*, 170.
(29) Hinrichsen, O.; Rosowski, F.; Hornung, A.; Muhler, M.; Ertl, G. *J. Catal.* **1997**, *165*, 33.
(30) Rekoske, J. E.; Cortright, R. D.; Goddard, S. A.; Sharma, S. B.; A., D. J. *J. Phys. Chem.* **1992**, *96*, 1880.
(31) Aparicio, L. M. *J. Catal.* **1997**, *165*, 262.
(32) Schmitz, G. *J. Chem. Phys.* **2000**, *112*, 10714.
(33) van de Runstraat, A.; van Grondelle, J.; van Santen, R. A. *Ind. Eng. Chem. Res.* **1997**, *36*, 3116.
(34) Aparicio, L. M.; Rossini, S. A.; Sanfilippo, D. G.; Rekoske, J. E.; Trevino, A. A.; Dumesic, J. A. *Ind. Eng. Chem. Res.* **1991**, *30*, 2114.
(35) Sellers, H.; Shustorovich, E. *Surf. Sci.* **2002**, *504*, 167.
(36) Benson, S. W. *Thermochemical kinetics: methods for the estimation of thermochemical data and rate parameters*, 2nd ed.; Wiley: New York, 1976.
(37) Goodson, D. Z.; Roelse, D. W.; Chiang, W.-T.; Valone, S. M.; Doll, J. D. *J. Am. Chem. Soc.* **2000**, *122*, 9189.
(38) Davis, H. T.; Thomson, K. T. *Linear Algebra and Linear Operators in Engineering: with Applications in Mathematica*; Academic Press: San Diego, CA, 2000.
(39) Aris, R.; Mah, R. *Ind. Eng. Chem. Fundam.* **1963**, *2*, 90.
(40) Gadewar, S. B.; Doherty, M. F.; Malone, M. F. *Comput. Chem. Eng.* **2001**, *25*, 1199.
(41) Masel, R. I. *Chemical Kinetics and Catalysis*; Wiley: New York, 2001; p 717.
(42) Horiuti, J.; Polanyi, M. *Trans. Faraday Soc.* **1934**, *30*, 1164.
(43) Bowker, M.; Parker, I.; Waugh, K. C. *Surf. Sci.* **1988**, *197*, L223.

(44) Bowker, M.; Parker, I. B.; Waugh, K. C. *Appl. Catal.* **1985**, *14*, 101.
(45) Dumesic, J. A.; Trevino, A. A. *J. Catal.* **1989**, *116*, 119.
(46) Stoltze, P.; Norskov, J. K. *J. Vac. Sci. Technol. A* **1987**, *5*, 581.
(47) Stoltze, P.; Norskov, J. K. *Surf. Sci.* **1988**, *197*, L230.
(48) Stoltze, P.; Norskov, J. K. *Phys. Rev. Lett.* **1985**, *55*, 2502.
(49) Stoltze, P.; Norskov, J. K. *J. Catal.* **1988**, *110*, 1.
(50) Ertl, G.; Lee, S. B.; Weiss, M. *Surf. Sci.* **1982**, *114*, 527.
(51) Dooling, D. J.; Rekoske, J. E.; Broadbelt, L. J. *Langmuir* **1999**, *15*, 5846.
(52) Masel, R. I.; Lee, W. T. *J. Catal.* **1997**, *165*, 80.
(53) Williams, W. R.; Marks, C. M.; Schmidt, L. D. *J. Phys. Chem.* **1992**, *96*, 5922.
(54) Coltrin, M. E.; Kee, R. J.; Rupley, F. M. *Surface Chemkin (version 4.0): A FORTRAN package for analyzing heterogeneous chemical kinetics at a solid-surface−gas-phase interface*; Sandia National Laboratories Report No. SAND90-8003B: Livermore, CA, 1991.
(55) Visual-Numerics *IMSL FORTRAN subroutines for mathematical applications*, 1997.
(56) Box, G. E. P.; Draper, N. R. *Empirical Model-Building and Response Surfaces*; Wiley: New York, 1987.
(57) van Santen, R. A.; Niemantsverdriet, J. W. *Chemical Kinetics and Catalysis*; Plenum Press: New York, 1995.
(58) Zhdanov, V. P. *Surf. Sci. Rep.* **1991**, *12*, 183.
(59) Davis, S. G.; Mhadeshwar, A. B.; Vlachos, D. G.; Wang, H. *Int. J. Chem. Kinet.*, accepted.
(60) Al-Muhtaseb, S. A.; Ritter, J. A. *J. Chem. Phys. B* **1999**, *103*, 8104.
(61) GRI *Gas-Research-Institute mechanism for natural gas (3.0)*; taken from http://www.me.berkeley.edu/gri_mech/, 1999.